Journal of Photochemistry and Photobiology A: Chemistry 252 (2013) 194–202

Contents lists available at SciVerse ScienceDirect

Journal of Photochemistry and Photobiology A: Chemistry

journal homepage: www.elsevier.com/locate/jphotochem

Fabrication of an optimized fluorescer encapsulated polymer coated gelatin nanoparticle and study of its retarded release properties

Deboleena Sarkar*

Unilever Research Center, 64 Main Road, Whitefield, Bangalore 560 066, India

ARTICLE INFO

Article history:
Received 3 September 2012
Received in revised form 31 October 2012
Accepted 21 November 2012
Available online 16 December 2012

Keywords:
Rhodamine B
Encapsulation
Myristoleic acid
Oleic acid
Gelatin
Nanoparticles

ABSTRACT

In this article the preparation and characterization of a fluorescent probe, rhodamine B, encapsulated gelatin nanoparticles has been described. The retardant release properties of the same have also been studied with its probable application in drug delivery systems. To decrease the release rate of the dye, fatty acid has been polymerized on the surface of the gelatin capsules or coacervates forming protective shells. The synthesis was carried out through the coacervation method with the aim to lead to the delayed release of the fluorescer from the gelatin polysaccharide matrix. The characteristics of fatty acids loading and chain length factors affecting their release from nanocapsules were investigated. The coacervated nanoparticles had uniform spherical shape with a size distribution of 195 ± 10 nm for nanoparticles formed with myristoleic acid precursor and at 160 ± 8 nm with oleic acid precursor. Based on spectroscopic studies it was found that the loading efficiency was approximately 0.4 μg/mg of nanoparticles for poly(myristoleic acid) and 0.7 μg/mg for poly(oleic acid). A higher efficacy for poly(oleic acid) is justified due to increase in hydrophobicity with increase in polymer chain length. For the first time, to the best of my knowledge, a *polymeric chain length efficacy-dependent* nanoparticle has been synthesized and non-invasively characterized. The nanoparticles were found to exhibit biocompatibility and affinity for cells, as demonstrated through fluorescence microscopy. In all the cases, the results clearly demonstrate the superiority of the encapsulated nanoparticles over bare organic fluorescent dye molecules which may be applied for probe-labeling in matters of sensitive target detection. Therefore, there is enormous potential to apply these newly developed fluorescent probe encapsulated nanoparticles in various bio-detection systems.

1. Introduction

Fashionable fluorescence techniques have contributed significantly today's science and technology. Fluorescence labeling techniques have been used extensively in both biological research and in clinical diagnosis. To achieve sensitive detections, there is an increasing demand for fluorescence labeling probes that are more intense and stable [1].

In this respect, biological nanoparticles developed for drug delivery systems as an alternative to liposome technology, in order to overcome the problems related to the stability of these vesicles in biological fluids and during storage have become highly demanding [2]. The nanoparticle technology used in recent years has great significance in improving the efficacy of the drugs. The nanoparticles fit into colloidal drug delivery systems, which offer advantages of drug targeting as well as the enhancement of the cellular uptake [3,4], which benefits from reduction of undesired toxic side effects of the free drugs [5]. With their easy accessibility in the body, nanoparticles can be transported via the circulation to different body sites [6], thus aiding in systematic treatments. Nanoparticles can be prepared from a variety of materials such as protein, polysaccharides and synthetic polymers. The choice of materials depends on several factors including (i) size and morphology of the nanoparticles; (ii) surface charge and permeability of the nanoparticle; (iii) degree of biodegradability, biocompatibility and cytotoxicity, and (iv) targeted drug loading and release profile. The huge demand of biopolymer nanoparticles lies in the fact that in addition to the general advantages of nanoparticles, biopolymer nanoparticles in particular offer several advantages, which include the ease of their preparation from well-understood biodegradable polymers and their high stability in biological fluids and during storage. Nanoparticles made of biodegradable polymers like proteins and polysaccharides can act as efficient drug delivery vehicles for sustained, controlled and targeted release, aiming to improve the therapeutic effects and also to reduce the side effects of the formulated drugs. Further, the use of biodegradable polymers as the actuating platform for nanoparticle-based drug delivery encourages the development of safe-engineered drug-delivery vehicles.

* Tel.: +91 080 39831051.
E-mail addresses: debbierims@yahoo.co.in, Deboleena.Sarkar@unilever.com

1010-6030/$ – see front matter © 2012 Elsevier B.V. All rights reserved.
http://dx.doi.org/10.1016/j.jphotochem.2012.11.010

Optical imaging is the latest trend in imaging-guided therapy that involves the detection of light photons transmitted through tissues. It can non-invasively monitor the progression of disease and therapy [7,8]. Conventional fluorophores such as fluorescent dyes, bioluminescent proteins and fluorescent proteins were used initially. But the recent advancements in the development of fluorescent nanoparticles (FNPs) have made them potential candidates for imaging-guided therapy and they have a lot of advantages over their predecessors [9]. Nano-encapsulation of the organic dyes makes them more stable and amplifies their signal considerably [10]. The NPs can be made of polymers like poly(D,L-lactic-co-glycolic acid) and polymethmyristoleic acid [11]. These NPs have been doped with many organic dyes like IRG-023 Cy5, fluorescein and rhodamine B isothiocyanate (RITC) [10–14]. Labeling of NPs with a combination of dyes has also been reported [15]. The organic dye-doped NPs are usually synthesized by two main methods namely the Stober method and the microemulsion method. The size varies from 2 to 200 nm and can be controlled [9]. The traditional label method could have only one or a few fluorophores to signal one bimolecular recognition event. The dyes can also be covalently conjugated to the nanoparticle, which also serve the purpose of controlled or delayed therapeutic release. However, there are a few advantages of physical encapsulation of the dye as compared to chemical conjugation. Firstly it can be assured that through encapsulation, the integrity of the dye or the drug is kept intact and it can be simply released as and when required. Also encapsulation involves simpler steps for preparation as compared to a complex synthetic step that might be required to covalently conjugate the dye. Since the dye or the drug remains undamaged, yet encapsulated, therefore, the dye-doped nanoparticles might contain hundreds to thousands of dye molecules, therefore, an intense fluorescence signal that is up to 30,000-fold better than that of a single organic fluorophores. This extreme brightness makes them especially suitable for ultrasensitive bioanalysis and negates the need for additional reagents or signal amplification steps. Secondly, polymers are used to help in retarding the rate of release of the dye molecules from its shell. These doped FNPs are found to be quite photostable. The photostability is mainly due to the polymer coating that prevents the penetration of oxygen, thereby reducing the bleaching [16]. These advantages indicated that dye molecules encapsulated in the nanoparticles have high stability and retains their optical activity, thus providing a viable route for various applications with unique properties, such as biochemical and bio-analytical applications and development of photo-switchable devices [17–20].

However, the biocompatibility of many of these currently available FNPs is not acceptable, thus limiting their applications in vivo. One approach to develop FNPs with excellent biocompatibility and easy combination with biomacromolecules is to load a fluorescent dye into a suitable natural biopolymer carrier. Such fluorescer-encapsulated NPs exhibit good biocompatibility and water solubility. Therefore universal bioconjugation strategies can be used for simply attaching biomolecules to them. In this respect, gelatin shows promising qualifications. Gelatin is a natural water-soluble macromolecule resulting from the heat dissolution and partial hydrolysis of collagen. Gelatin offers a number of advantages over other synthetic polymers including non-irritability, biocompatibility and biodegradability, which makes it one of the desirable materials as carrier molecule [21,22]. It is a natural macromolecule which is non-toxic and non-carcinogenic, and it shows low immunogenicity and antigenicity [23,24]. Gelatin has large number of functional groups on its surface which aid in chemical crosslinking and derivatization. These advantages led to its application in the synthesis of nanoparticles for drug delivery during the last thirty years [25]. Thus, being motivated by the application potential of gelatin in biomedical and pharmaceutical fields, the preparation, characterization of a fluorescer encapsulated gelatin nanoparticle and its possible application for targeted therapeutic delivery seems to be exciting and relevant.

Nevertheless, due to the existence of cross-linkage of peptide side chains in gelatin nanoparticles, small pores or gaps are found on the nanoparticles surface, which leads to the leakage of encapsulated materials and instability especially for water soluble dyes or drugs [20]. This limits the application for the fluorescent gelatin nanoparticles. To overcome this problem, a different method of synthesis needs to be engineered to prepare a fluorescer encapsulated gelatin nanoparticle. Here rhodamine B (RhB) has been used as a choice of the fluorescent molecule. Furthermore, the gelatin nanospheres have been poly-fatty acid coated to retard the release of encapsulate. Experiments have been performed with in situ polymerized myristoleic acid and oleic acid, which have varying chain lengths, to suit our purpose. The strategy involves, mixing of the fatty acids into the gelatin and formation of the nanoparticles, in the presence of RhB, exploiting the coacervation method using sodium sulfate as the coacervation reagent [11]. The polymers are slowly cross-linked by formaldehyde under a mild condition with the help of an initiator. The RhBGNPs formed through this process enables a coating on the gelatin, thereby masking or blocking small pores or gaps. Thus the obtained RhBGNPs are expected to show a uniform spherical shape and excellent absorption and fluorescence properties. The retardant dye releasing capability, as well as the biocompatibility of the synthesized RhBGNPs has been checked. Thus the paper reports a complete synthesis, characterization and bioapplicability of RhBGNPs. Also the effective parameters of its manufacture such as temperature, gelatin concentration and coacervation agent effect have been discussed.

2. Materials and methods

2.1. Materials

Gelatin (Type B, isoelectric point 4.0–5.7), Tween-20 and sodium sulfate were purchased from S.D. Fine Chem. (India) and used as received. Rhodamine B and azobis 2-methylpropionamidine dihydrochloride (AIBA) were purchased from Aldrich Chemical Co., (USA). Myristoleic acid, oleic acid, formaldehyde (37%), isopropanol, and analytical grade sodium hydroxide were procured from E-Merck (India). Keratinocyte growth medium (KGM) was purchased from GIBCO, USA. A 10KD dialyzer was purchased from Thermo Scientific (USA). All the chemicals and solvents were used without further purification. Millipore water obtained from a Milli-Q purification system was used in entire process.

2.2. Preparation of RhBGNP

RhBGNPs were synthesized by coacervation method with sodium sulfate, followed by phase separation with isopropanol. The polymers were crosslinked with formaldehyde using a suitable initiator AIBA [11]. Briefly, 5 mg rhodamine B (Scheme 1a) was dissolved in 10 mL distilled water to which 500 mg sodium hydroxide, and 250 mg gelatin was added under continuous stirring for 10 min at 300 rpm at 50 °C. To this reddish pink solution, 500 μL of fatty acid (myristoleic acid or oleic acid) (Scheme 1b and c) followed by 100 μL of Tween-20 were added dropwise. After stirring the solution for about 5 min, 20% (w/w) sodium sulfate solution was added dropwise to the mixture whereby the solution was found to change from transparent to opaque indicating formation of a precipitate. 400 μL isopropanol was added to the solution while maintaining the temperature at 50 °C under continuous stirring for phase separation to take place. Next, 4.0 mL formaldehyde was introduced to the mixture as a cross-linking reagent and the solution was stirred

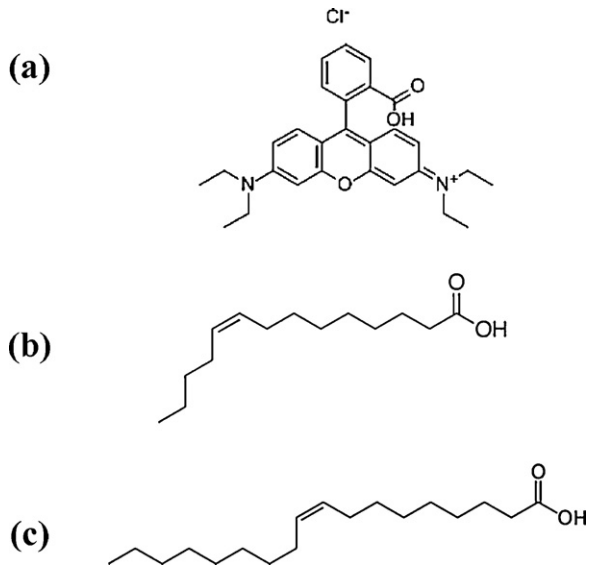

Scheme 1. Chemical structures of (a) rhodamine B, (b) myristoleic acid and (c) oleic acid.

for 30 min. Finally 50 mg AIBA was added as an initiator and the temperature of the system was raised to 60 °C. The mixture was maintained at this temperature for 6 h with continuous stirring to produce a nice dark red to pink fluorescent RhB encapsulated fatty acid coated gelatin nanoparticles as desired. The final product was dialyzed in a magnetic stirrer under slow stirring with Millipore water for 4 days to remove the free rhodamine B and other unreacted reagents. It has been observed and discussed in later section (Section 3.4), that after the beginning of the dynamic dialysis, the rhodamine B contents in the release medium were increased dramatically within 50 h for all three solutions after which it was slowed and saturated by a gradual and sustained release up to 60% in 80–90 h. Therefore a cut off of 4 days was chosen, after which a very slow release or rather saturation in the release was observed, to be on the safer side. The obtained RhBGNP nanoparticles were filtered through a 200 nm filtration membrane and stored at 4 °C prior to use. For solid state analysis, the RhBGNPs were lyophilized into powder prior to use.

Scheme 2 is a cartoon of the work that has been projected in the article and it shows the synthetic steps in a simplistic manner.

2.3. Instruments used

Scanning electron microscope (*SEM*). The morphology of the RhBGNP was investigated using a scanning electron microscope (SEM, Hitachi S-4700) with an accelerating voltage of 5 kV. Samples were mounted on holey carbon tape and imaged after gold sputter to make them conductive.

Transmission electron microscope (*TEM*). The TEM images were taken using a JEOL-TEM-2010 high resolution transmission electron microscope at an operating voltage of 200 kV.

Fourier transform infra red (*FT-IR*) *spectra*. Room temperature Fourier transform IR (FT-IR) measurements were performed on a Perkin-Elmer FT-IR spectrophotometer, Spectrum-100, using KBr pellet. For performing the IR studies, the dialyzed nanoparticles were lyophilized to powdered texture. To make a clear comparison, the IR spectra of gelatin and the individual fatty acid were also taken. The spectra were normalized and separated for the convenience of comparison.

Dynamic light scattering (*DLS*). DLS measurements were performed on a Brookhaven Instrument (BI 2000) equipped with an autocorrelator (BI-9K) and goniometer (BI-200SM) with a BIHV photomultiplier tube. An argon ion laser (LEXEL 95-2) operating at 488 nm was used as the light source. The beam was focused onto the sample cell (standard cylindrical 4.5 mL cuvettes) through a temperature-controlled chamber (the temperature was controlled within 23 ± 0.1 °C). All experiments were done at a correlation time of 2 min. The measurements were carried out at 90°. The available software records the autocorrelation of the intensity trace during the experiment. Once the autocorrelation data have been generated, the averaged translational diffusion coefficient of the sample is derived mathematically from the fitting parameter, the average decay rate, and the scattering vector at a given angle of 90°. The hydrodynamic radius, R_H, is computed on the basis of the Stokes–Einstein equation. The average hydrodynamic radius was obtained from three individual measurements for each system.

UV–vis absorption and fluorescence spectroscopy. All fluorescence studies were performed using a Shimadzu RF-5301PC fluorimeter with excitation and emission slits both set to 3.0 nm. UV–vis absorption spectra were measured on Perkin-Elmer Lambda-35 spectrophotometer with properly corrected background using Millipore water.

To calculate the concentration of the nanoparticles, it was assumed that the molar extinction coefficient (ε) of nanoparticles containing rhodamine B had no change compared with the

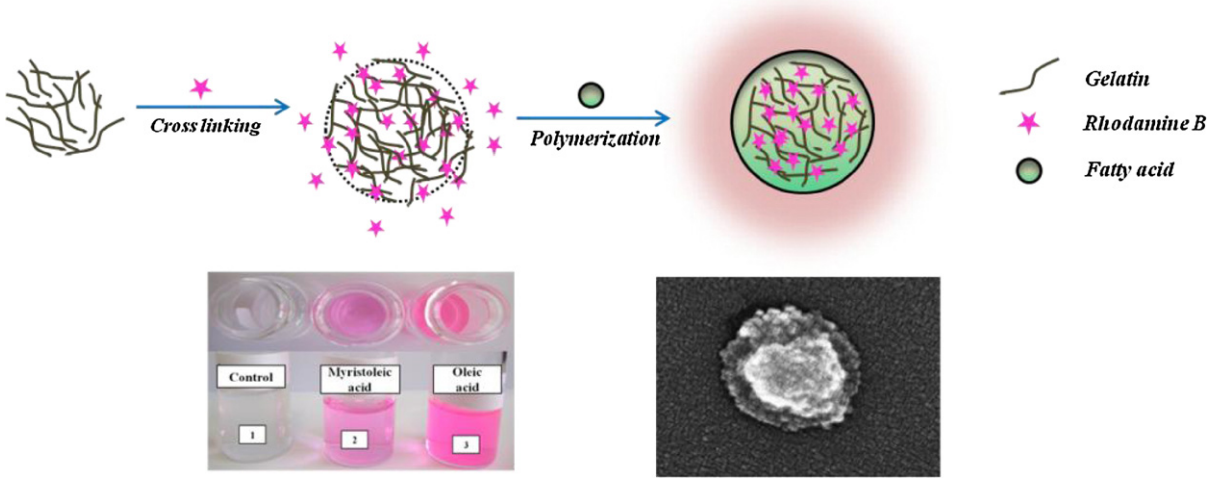

Scheme 2. Schematic illustration for the preparation of the RhBGNP nanoparticles.

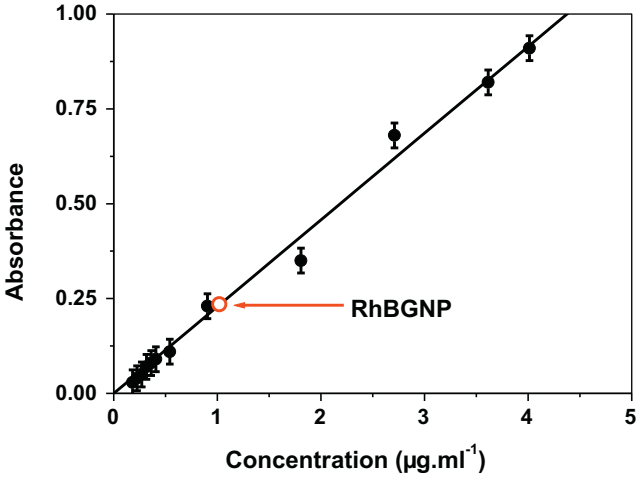

Fig. 1. Calibration curve generated to estimate the concentration of the synthesized nanoparticle.

rhodamine B dissolved in distilled water. Thus, a series of rhodamine B aqueous solution with different concentrations were used as calibration (which covered three orders of magnitude from 4.0 ng mL^{-1} to 4.0 μg mL^{-1}) and the concentration of the known amount of synthesized nanoparticle added to a known volume of water was obtained by interpolating the OD value of this test solution on to this calibration curve. To compare its spectral behavior to rhodamine B, an aqueous solution of rhodamine B was prepared, the concentration of which was kept similar to that of the nanoparticle (Fig. 1).

The entrapment efficiency of nanoparticles was determined by the method proposed by Vandervoort and Ludwig [26]. The amount of un-entrapped drug was determined spectrophotometrically assuming that the molar extinction coefficient (ε) of encapsulated rhodamine B does not change compared with the rhodamine B dissolved in distilled water.

$$\text{Dye entrapment}\,(\%) = \frac{(\text{amount of dye used in formulation} - \text{amount of unbound dye}) \times 100}{\text{amount of dye used in formulation}}$$

The in vitro retardant dye release of the RhBGNPs was studied through the dynamic dialysis method for the measurement of release of encapsulated rhodamine B. Briefly the newly prepared nanoparticles suspension was syringed and placed into a dialysis bag (10 kD). The bag was then clipped onto holders and put into a glass beaker containing 1000 mL of Millipore water with magnetic stirring at 200 rpm and 25 °C. At regular time intervals, 2 mL of release medium was withdrawn, and the rhodamine B content was determined by UV–vis absorption spectra at wavelength of 555 nm. Same protocol was followed for the nanoparticles prepared in a similar fashion but without fatty acid and presented for comparison.

Fluorescence microscopy. To demonstrate the cellular uptake results of the synthesized nanoparticles, fluorescence images of the nanoparticle-labeled cells were observed by fluorescence microscope (Olympus BX40, Japan) at room temperature.

For the cellular studies, primary keratinocytes cell line was used. To the cultured cells, 100 mg mL^{-1} of prepared nanoparticle suspension in PBS buffer was added. It was then suspended in the growth medium and plated in tissue culture flasks and incubated at 37 °C, 5% carbon dioxide for 2 h. After 2 h incubation, they were washed with the growth medium four times and fixed in 4% paraformaldehyde, stained with nucleus staining probe, 4′,6-diamidino-2-phenylindole (DAPI) and imaged in the fluorescence microscope.

3. Results and discussion

3.1. Fabrication of RhB encapsulated gelatin nanoparticles

The preparation method for RhBGNP involved the process of coacervation with sodium sulfate, followed by phase separation using isopropanol, cross-linking by formaldehyde, and polymerization initiated by AIBA. The nanoparticles prepared thus were found to be highly stable in water as well as in the cell medium. This method leads to the formation of least aggregated particles with uniform distribution [11]. The process was judiciously carried out with fatty acid polymerized in situ so that a polymeric layer was formed on the encapsulated dye thereby retarding its release in a hydrogel drug delivery system [11]. In short the polymerized fatty acid helped in forming a protective layer at the surface of gelatin nanoparticles. The preparation was carried out at an alkaline pH, which was required by the crosslinking reaction of gelatin nanoparticles using formaldehyde as the cross-linking reagent. Continuous dialysis was carried out finally to remove the free rhodamine B and other unreacted reagents and to bring down the pH to neutral which could retard the release of encapsulated rhodamine B from the nanoparticles. In a number of reports, different synthesis parameters that most affect nanoparticle size have been investigated [27–29]. It is obvious that preparation of nanoparticles at low temperature was not possible due to the fact that gelatin forms highly viscous gel. However, increasing the temperature above 50 °C increases the particle size which is due to the gelling properties of gelatin at higher temperatures. The triple helical structure is found to uncoil when the temperature greatly increases since viscosity decreases simultaneously. At 50 °C, the chains seem to be sufficiently uncoiled and the addition of the desolvating agent causes a better controlled precipitation of the macromolecules. Also it is pertinent to mention that if the reaction temperature is too high, the organic dye encapsulated in the nanoparticles may be decomposed. Given all these concerns, the reaction temperature in the present study was thus set to 50 °C at the mixture step and raised to 60 °C for the polymerization. Under this delicate condition AIBA helps in polymerization by acting as an initiator. AIBA is a widely used blowing agent and initiator and is a typical self-reactive material. It is basically a free radical-generating azo compound. Whereas mechanism of polymerization with azo-initiators is not well understood, it is assumed that since AIBA is a water soluble highly reactive initiator, it gives clean reaction in a short time without drastic conditions.

In the present case, formaldehyde was chosen over glutaraldehyde as the cross-linking agent, which is generally more common. It is known that glutaraldehyde forms a dark-yellow solution with amino acid and in the present study this deep color was found to interfere with the red color of RhB which gives erroneous results in absorption and fluorescence experiments. Formaldehyde being colorless was therefore used to circumvent the problem, yet function as the crosslinker. Formaldehyde is known to react with several peptide side chain groups, especially lysine residues along the gelatin chain in order to form a methylene bridge or a crosslinkage. Therefore, upon using formaldehyde the cross-linking reaction could be completed and the final RhBGNP nanoparticle product could remain transparent, which helps in the spectroscopic characterization of the encapsulated rhodamine B. The optimized pH range for the cross-linking of formaldehyde was found to be 8–9. Thus, the pH of the reaction was carefully adjusted in the mixing step with just enough sodium hydroxide to neutralize the added acid.

Maintaining all these conditions, the polymerization could be coacervated by sodium sulfate, initiated by the AIBA, crosslinked by formaldehyde, and the formation of RhBGNP could be completed in 6 h. Visually it could be seen that the nanoparticles formed with oleic acid gave a brighter and a slightly deeper shade of pink with the same amount of rhodamine B compared to that with myristoleic acid (Fig. 2).

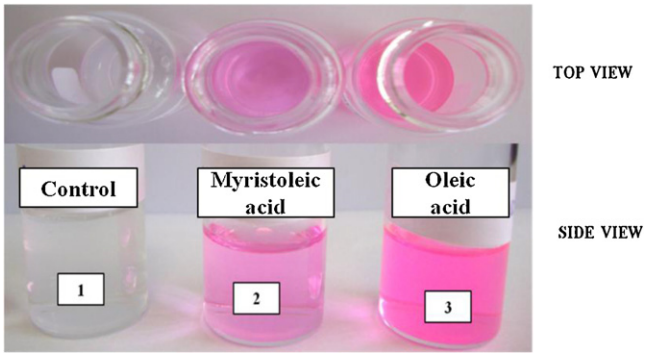

Fig. 2. A snapshot of the three vials containing (1) gelatin nanoparticles with myristoleic acid in absence of RhB, (2) gelatin nanoparticles with myristoleic acid in presence of RhB, and (3) gelatin nanoparticles with oleic acid in presence of equivalent amount of RhB.

3.2. Morphology analysis and physical characterization

3.2.1. Scanning electron microscopy (SEM), transmission electron microscopy (TEM) and dynamic light scattering (DLS) studies

The SEM image of synthesized RhBGNP is shown in Fig. 3. A close-up of the nanoparticle shows that they are spherical in nature with an average diameter of ~200 nm. This value was also confirmed through DLS measurements. The photograph clearly indicates that no hairline cracks or heterogeneity appear on the nanoparticles surface. This obviously presents morphological evidence for solid and smooth nanoparticles. From the figure, two layers are observed, the core possibly being the gelatin nanoparticles with a shell of polymerized fatty acid coating. We have used TEM data to further substantiate this result (Fig. 3c).

In many of the reports the gelatin nanoparticles were found to have a diameter between 250 and 300 nm [28–30]. DLS studies were performed to find out the actual diameter of the nanoparticles and their dispersity in solution. Through the coacervation method, the diameters of the gelatin nanoparticles were controlled at around 195 nm for RhBGNP formed with myristoleic acid and at about 161 nm for RhBGNP formed with oleic acid by the amount of added inorganic coacervation reagent, as confirmed by the DLS experiments (Fig. 4).

A lower hydrodynamic diameter for RhBGNP formed with oleic acid as compared to that with myristoleic acid shows that smaller particles are formed with the former. The diffusion coefficient simulated from the software was found to be 2.27×10^{-8} cm^2 s^{-1} for myristoleic acid and 4.32×10^{-8} cm^2 s^{-1} for oleic acid, indicating finer particles formed for oleic acid. This may be due to better encapsulation of RhB in oleic acid due to longer hydrophobic chain length in oleic acid compared to myristoleic acid. With more sodium sulfate added, the diameter of the nanoparticles was found to increase. Moreover, a higher temperature or longer reaction time for the crosslinking also led to increase in the diameter. Use of hydrophobic solvent helps in avoiding the washing step and therefore makes the synthesized nanoparticles more compatible for biochemical applications.

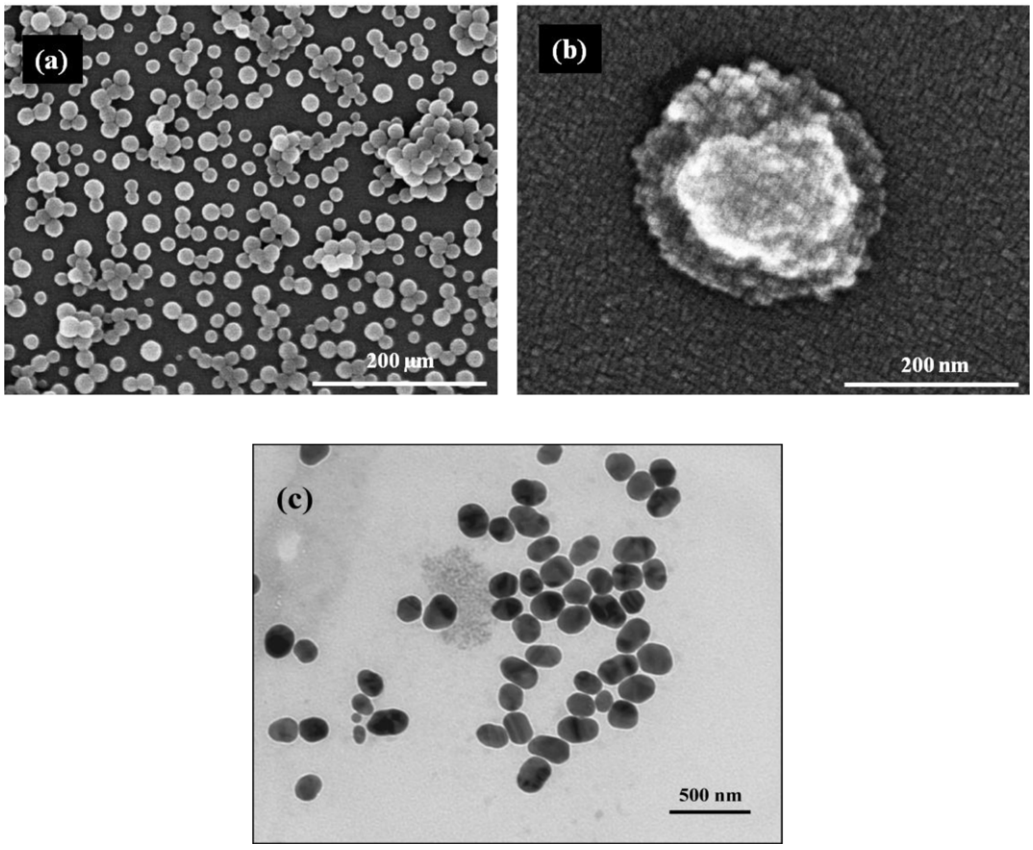

Fig. 3. (a) and (b) SEM image and (c) TEM image of RhBGNP with myristoleic acid.

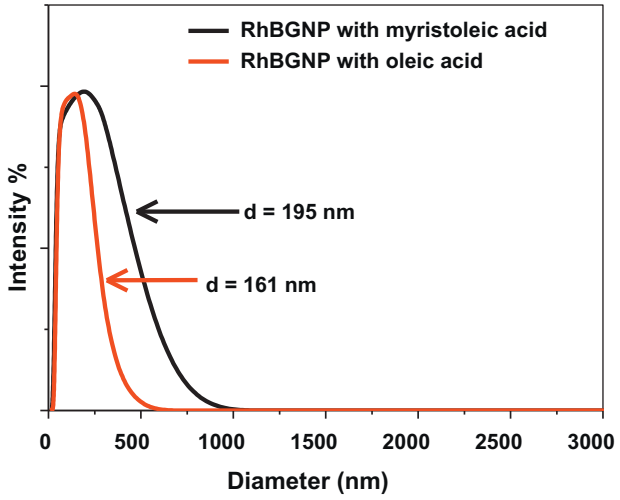

Fig. 4. Size distribution graph for RhBGNP formed with myristoleic acid and oleic acid. Solutions were made in water with nanoparticle concentration of 1 μg mL^{-1} in both the cases.

3.2.2. IR spectra of RhBGNP nanoparticles

Fig. 5 shows the IR spectra of gelatin, fatty acid and the synthesized nanoparticles on the same chart. From the IR spectra, the moderate stretching vibration of the N—H bond can be observed around 3300 cm^{-1} for the synthesized nanoparticles vis-à-vis the IR spectra of gelatin which reveals the existence of amide in both the synthesized nanoparticles [31]. C—H bond stretching shows its signature at ~2900 cm^{-1} in both the fatty acid as well as the synthesized nanoparticles proving that the integrity of the nanoparticles is preserved in all manners. The fingerprint region of carbonyl groups at 1650–1700 cm^{-1} shows the presence of the same in both the synthesized nanoparticles, derived from the carboxyl group of fatty acid. Therefore, from the IR spectra a strong conclusion regarding the formation of RhB nanoparticles formed from fatty acid coated onto the gelatin matrix could be vividly drawn. It further substantiates the applicability of the synthesis procedure used for fabricating these nanoparticles. As a control, an RhBGNP without the fatty acids was also prepared and an IR scan for the same was also taken (figure not shown). The fingerprints of the control nanoparticle resembled

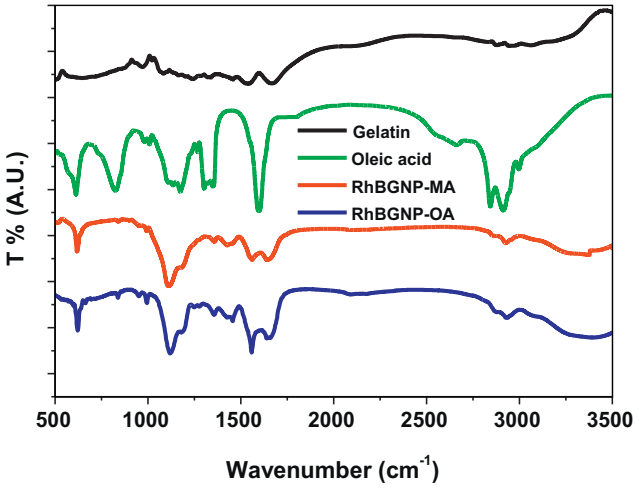

Fig. 5. IR spectra of gelatin, oleic acid, RhBGNP with myristoleic acid (RhBGNP-MA) and RhBGNP with oleic acid (RhBGNP-OA). The % transmission of all the spectra were normalized and separated for the convenience of comparison. The spectrum of only myristoleic acid has been omitted to provide a visual clarification.

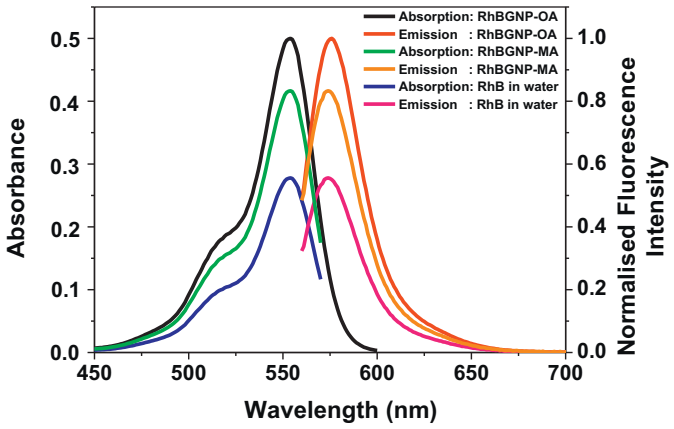

Fig. 6. Absorption and normalized fluorescence spectra of RhB encapsulated nanoparticles with myrisoleic acid (MA) and oleic acid (OA) compared with that of RhB aqueous solution. The effective concentration of dye in all the solutions has been kept at 1 μg mL^{-1}.

that of bare gelatin only and, as expected, had no features of the fatty acids. The fact that, in case of the RhBGNPs prepared in presence of fatty acid shows fingerprints of both gelatin as well as the precursor acid is a proof of the fact that the particles have been polymer coated which is also seen through SEM.

3.3. Spectral analysis: absorbance and fluorescence

Rhodamine B is known to absorb at ~555 nm in bulk aqueous medium and shows a broad, intense emission at ~575 nm which are almost mirror images of each other [32]. The absorption and emission peak of encapsulated rhodamine B nanoparticles were found to have no significant shift in position compared to the free rhodamine B dissolved in water (Fig. 6).

This implies that the synthesized nanoparticles are transparent and have no effect on the optical behavior of the encapsulated dye. The nanoparticle, thus, have been synthesized through such a non-invasive procedure that restores the integrity of the dye even in its encapsulated form. The concentration of all the solutions were so adjusted that in each of them the effective dye concentration was 1 μg mL^{-1} to eliminate any anomaly due to differential loading. The nanoparticle solutions were sonicated for about 30 min prior to performing the experiments to ensure complete and homogeneous solution.

The most apparent observation from the spectral features in Fig. 6 is the fact that both the RhB encapsulated nanoparticles had reasonably strong emission intensity and higher fluorescent yield compared to that of the same amount of RhB in water, which indicates that not only the nanoparticles were transparent for the encapsulated dye to demonstrate its optical behavior but also they could provide a suitable environment for the dye molecules to be concentrated at a certain location leading to high emission efficiency. This protection and concentration through encapsulation of RhB provided by the nanoparticles therefore results in enhanced emission intensity with equivalent dye concentration compared to the rhodamine B aqueous solution, which could be used for higher sensitive fluorescence tracing in the future. The pH effect on the fluorescence intensity on the encapsulated nanoparticles was also carried out by using PBS buffer (pH = 6.0, 7.0, 8.0, and 9.0, respectively). The fluorescence intensities of these serial solutions had no significant differences (data not shown).

The other important fact is that the absorption and fluorescence spectra in Fig. 6 clearly shows that the synthesized nanoparticles from oleic acid are more fluorescent and have higher absorbance

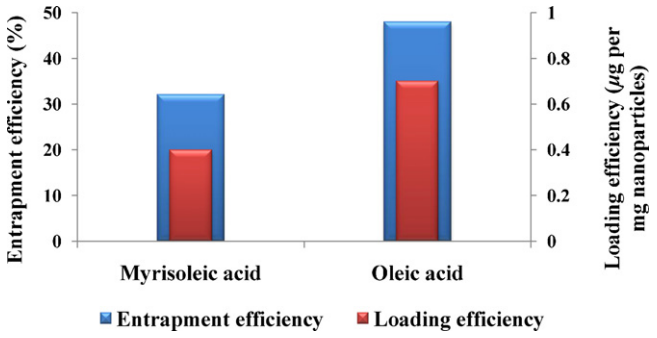

Fig. 7. Comparison of entrapment efficiency and loading efficiency of RhB encapsulated in the nanoparticles formed individually from myristoleic acid and oleic acid.

compared to that obtained from myristoleic acid at the same concentration of the encapsulated dye, which is also evident from Fig. 2. This indicates that is better and efficient encapsulation of the dye in the nanoparticles formed from a longer chain fatty acid, i.e., oleic acid. It implies that the longer chain fatty acid provides a more hydrophobic environment and helps in protecting the dye more efficiently thereby forming a secured dye encapsulated nanoparticle which is more optically active than that formed from a shorter chain fatty acid. Therefore, for the first time, to the best of my knowledge, a dye-encapsulated fatty acid coated gelatin nanoparticle has been synthesized non-invasively whose efficacy is found to depend on the polymeric chain length. This will help one to tune the behavior and performance of the nanoparticle to ones desire by just controlling the chain length of the starting fatty acid.

3.4. Entrapment efficiency and in vitro dye release through encapsulation within nanoparticles

Entrapment efficiency was calculated according to the equation in Section 2.3. Taking the initial amount of dye used to prepare the formulations to be 5 mg for both the cases, it is found that the percentage of dye entrapment comes out to be 32% for nanoparticles with myristoleic acid and 48% for the nanoparticles with oleic acid (within a ±1% error limit). Therefore oleic acid shows a greater efficiency in entrapping the dye in its core shell as compared to myristoleic acid. The advantage of oleic acid lies in its longer chain length which gives better encapsulation and better protection to the dye and leads to higher efficiency.

Further, a certain volume of the synthesized nanoparticles solution was lyophilized, and the powder was weighed. The rhodamine B loading efficiency in the nanoparticles was thereby found to be 0.4 ± 0.02 μg/mg of nanoparticles for myristoleic acid and 0.7 ± 0.03 μg/mg of nanoparticles for oleic acid. This further substantiates quantitatively a higher efficacy of encapsulation in case of long chain polymer oleic acid as compared to that for short chain polymer myristoleic acid (Fig. 7).

The in vitro retardant dye release of the RhBGNPs was studied through the dynamic dialysis method for the measurement of release of encapsulated rhodamine B as described in Section 2.3. It was observed that in the first 20 h almost 20% of RhB was released from the nanoparticles, which increased to ~40% in 50 h. So, after the beginning of the dynamic dialysis, the rhodamine B contents in the release medium were increased dramatically within 40 h for all three solutions after which it was slowed and saturated by a gradual and sustained release up to 60% or even less to ~40% in 80 h (Fig. 8).

The release behavior of dye from the gelatin matrix showed a biphasic pattern that is characterized by an initial burst, followed by a sustained release. The initial-burst release may have occurred

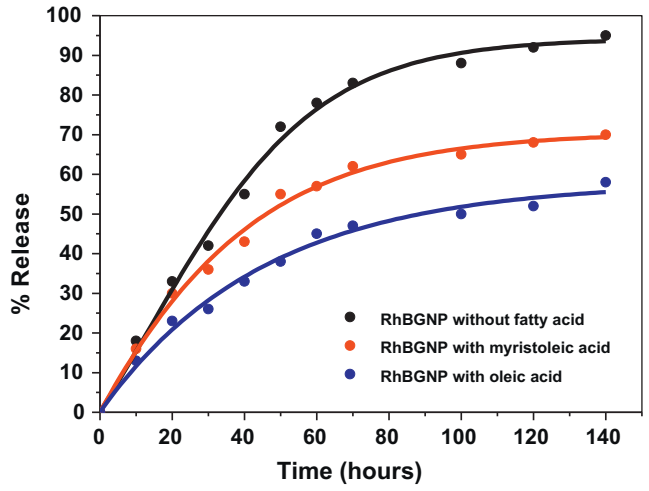

Fig. 8. Dynamic dialysis release curve of RhBGNPs formed with myristoleic acid and oleic acid coating. Gelatin nanoparticles formed without fatty acid coating have also been presented in the same graph for comparison. See legends for details. Millipore water was used as dialysis medium.

due to the release of dye present at or just beneath the surface of the nanoparticles. Then, release may have occurred due to the diffusion of dye molecules through the polymeric matrix of the nanoparticles. Therefore, after 50 h dialysis, the increased rhodamine B content in the release medium was contributed to the release of encapsulated rhodamine B. The biphasic release was found to be similar to that previously reported by other research groups [33–35]. As comparison and control, the release profile of gelatin nanoparticles without fatty acid coating showed a faster release of encapsulated rhodamine B with a release percentage around 80% after 60 h dialysis, which indicated that the polymerization of fatty acid helps in protecting rhodamine B. It shows a retardant release property compared to the gelatin nanoparticles without fatty acid coating. This furthermore establishes the existence of the fatty acid coating on the nanoparticles which is enabling a slow-release of RhB. Also the retardant release of RhBGNP with oleic acid coating was found to be more effective as compared to that with myristoleic acid which further substantiates the fact that oleic acid provides a better protection owing to its longer chain as compared to myristoleic acid which thereby protects the encapsulated dye from release for a longer period of time, effectively. The retardant dye release property, thus, indicates that the fatty acids, which combined into the gelatin matrix and formed a coating layer on the gelatin nanoparticles, had a protective effect because it can block the pores on the surface of gelatin nanoparticles and thus delay the release of encapsulated rhodamine B. This elongated release time of the synthesized nanoparticles could be used for biochemical and bioanalytical applications in the future.

Overall, the results demonstrate the advantages of the encapsulated nanoparticles over bare organic fluorescent dye molecules in terms fluorescent brightness and releasing time. Though it is difficult to estimate the amount of dye present in a single nanoparticle, it is possible to quantify the percentage of dye entrapment and the loading amount as shown above.

3.5. Fluorescence imaging analysis

For the cellular studies, primary keratinocytes cell line was used. Keratinocytes are the first line of defense against any chemical exposure. It has been shown that keratinocytes are capable of antigen presentation and may be used as a model to differentiate between contact allergen and irritants [36,37]. Contact dermatitis is a skin inflammatory response caused by direct contact with

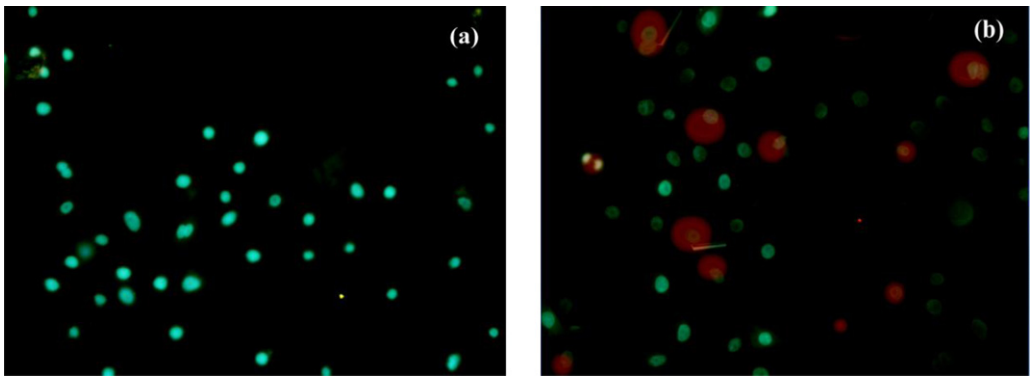

Fig. 9. Fluorescence imaging of primary keratinocytes cells with DAPI staining incubated (a) without RhBGNP and (b) with RhBGNPs prepared from oleic acid.

a chemical substance. This can be broadly classified as allergic contact dermatitis and irritant contact dermatitis. Irritant contact dermatitis is a T-cell independent local skin inflammatory response induced by a chemical substance whereas allergic contact dermatitis is a delayed T-cell dependent response that requires a previous sensitization by the allergen molecule [38,39]. Therefore, to study epidermal homeostatic control mechanisms, the epidermal cells (keratinocytes) serve as an excellent model.

The fluorescence microscope image is displayed in Fig. 9. The reds in the figure suggests uptake of the nanoparticles into the nucleus. This property of RhBGNPs possibly results from the small size of the nanoparticles. However, the nanoparticles did not distribute uniformly in the cell, as can be seen from Fig. 8. This could be attributed to the different affinity of the organelle to the synthesized nanoparticles.

4. Conclusion

Nanoparticle-based delivery systems have the potential power to improve drug stability, increase the duration of the therapeutic effect and permit enteral or parenteral administration, which may prevent or minimize the drug degradation and metabolism as well as cellular efflux. In this context, gelatin nanoparticles are very well known as active drug delivery or gene delivery vehicles because they can easily direct and control gene expression kinetics. Furthermore, surface modification of gelatin nanoparticles, by covalent attachment of a polymer or a biopolymer, is one of the efficient and clever strategies employed to meet specific controlled release needs due to their versatility in chemical modification and crosslinking. In this paper, such kind of a surface modification of gelatin nanoparticles has been done with fatty acid polymers. Rhodamine B encapsulated fatty acid polymer coated gelatin nanoparticles has been prepared using an improved coacervation and phase separation method with formaldehyde as a cross-linking reagent at 60 °C. The nanoparticles have been characterized through SEM, IR and DLS studies. The coating of polymer layer on the surface of gelatin nanoparticles has been also confirmed. Through spectroscopic studies, the delayed release of RhB from the gelatin nanoparticle has been estimated. Further, it has been shown that the chain length and the hydrophobicity of the precursor fatty acid plays a governing role in the efficacy and the delayed release ability of the synthesized nanoparticles. Oleic acid based RhBGNPs showed a slower release and a better loading efficacy compared to myristoleic acid based RhBGNPs owing to a longer alkyl chain length of the former. Finally fluorescence imaging studies with primary keratinocytes suggests uptake of the nanoparticles into the nucleus which proved that the synthesized nanoparticles are biocompatible.

Acknowledgements

The author thanks Mr. Somnath Das, Mr. Sumit Ghosh and Dr. Amitabha Majumdar, of Unilever R&D Bangalore for their help in certain experiments and Dr. Amitava Pramanik for helpful discussions.

References

[1] W. Lian, S.A. Litherland, H. Badrane, W. Tan, D. Wu, H.V. Baker, P.A. Gulig, D.V. Lim, S. Jin, Analytical Biochemistry 334 (2004) 135–144.
[2] M.T. Heemels, Nature 407 (2000) 769.
[3] I.L. Medintz, H.T. Uyeda, E.R. Goldman, H. Mattoussi, Nature Materials 4 (2005) 435–446.
[4] K.H. Wagenheim, H.P. Peterson, Journal of Theoretical Biology 193 (1998) 663–678.
[5] B.R. Gastman, Head and Neck 23 (2001) 409–425.
[6] H.J. Guchelaar, A. Vermes, I. Vermes, C. Haanen, Pharmacy World and Science 19 (1997) 119–125.
[7] D. Sarkar, D. Bose, A. Mahata, D. Ghosh, N. Chattopadhyay, Journal of Physical Chemistry B 114 (2010) 2261–2269.
[8] D. Sarkar, P. Das, S. Basak, N. Chattopadhyay, Journal of Physical Chemistry B 112 (2008) 9243–9249.
[9] S. Jiang, M.K. Gnanasammandhan, Y. Zhang, Journal of the Royal Society Interface 7 (2010) 3–18.
[10] D. Ghosh, D. Sarkar, A. Girigoswami, N. Chattopadhyay, Journal for Nanoscience and Nanotechnology 11 (2011) 1141–1146.
[11] Z. Gan, J. Ju, T. Zhang, D. Wu, Journal of Nanomaterials 2011 (2011) 1–8.
[12] Y. Liu, S. Zha, M. Liu, Advanced Materials 16 (2004) 256–260.
[13] X.X. He, J.Y. Chen, K.M. Wang, D.L. Qin, W.H. Tan, Talanta 72 (2007) 1519–1526.
[14] H. Shi, X.X. He, K.M. Wang, Y. Yuan, K. Deng, J.Y. Chen, W.H. Tan, Nanomedicine: Nanotechnology, Biology and Medicine 3 (2007) 266–272.
[15] L. Wang, C.Y. Yang, W.H. Tan, Nano Letters 5 (2005) 37–43.
[16] X.C. Zhou, J.Z. Zhou, Analytical Chemistry 76 (2004) 5302–5312.
[17] W. Yang, C.G. Zhang, H.Y. Qu, H.H. Yang, J.G. Xu, Analytica Chimica Acta 503 (2004) 163–169.
[18] Z. Tian, W. Wu, A.D.Q. Li, ChemPhysChem 10 (2009) 2577–2591.
[19] F. Wang, W.B. Tan, Y. Zhang, X. Fan, M. Wang, Nanotechnology 17 (2006) R1–R13.
[20] A. Burns, H. Ow, U. Wiesner, Chemical Society Reviews 35 (2006) 1028–1042.
[21] H.G. Schwick, K. Heide, Bibliotheca Haematologica 3 (1969) 111.
[22] A.G. Ward, A. Courts, The Science and Technology of Gelatin, Academic Press, New York, 1977.
[23] A.K. Bajpai, J.J. Choubey, Journal of Materials Science Materials in Medicine 17 (2006) 345–358.
[24] Y. Marios, N. Chakfe, X. Deng, M. Marios, T. How, W. King, R. Guidoin, Biomaterials 16 (1995) 1131–1139.
[25] J. Kreuter, Pharmaceutica Acta Helvetiae 53 (1978) 33–39.
[26] J. Vandervoort, A. Ludwig, European Journal of Pharmaceutics and Biopharmaceutics 57 (2004) 251–261.
[27] G.K. Saraogi, P. Gupta, U.D. Gupta, N.K. Jain, G.P. Agrawala, International Journal of Pharmaceutics 385 (2010) 143–149.
[28] M. Jahanshahi, S. Williams, A. Lyddiatt, S.A. Shojaosadati, IEE Proceedings Nanobiotechnology 151 (2004) 176–182.
[29] T.G. Shutava, S.S. Balkundi, P. Vangala, J.J. Steffan, R.L. Bigelow, J.A. Cardelli, D.P. O'Neal, Y.M. Lvov, ACS Nano 3 (2009) 1877–1885.
[30] M. Jahanshahi, M.H. Sanati, S. Hajizadeh, Z. Babaei, Physica Status Solidi A 205 (2008) 2898–2902.
[31] K.J. Payne, A. Veis, Biopolymers 27 (1988) 1749–1760.
[32] K. Garai, R. Sureka, S. Maiti, Biophysical Journal 92 (2007) L55–L57.
[33] A.K. Verma, K. Sachin, A. Saxena, H.B. Bohidar, Current Pharmaceutical Biotechnology 6 (2005) 121–130.

[34] E. Leo, R. Cameroni, F. Forni, International Journal of Pharmaceutics 180 (1999) 23–30.
[35] M. Nahar, D. Mishra, V. Dubey, N.K. Jain, Nanomedicine: Nanotechnology, Biology and Medicine 4 (2008) 252–261.
[36] G. Banerjee, A. Damodaran, N. Devi, K. Dharmalingam, G. Raman, Scandinavian Journal of Immunology 59 (2004) 385–394.
[37] M. De Bueger, A. Balder, E. Goulmy, Immunology 1 (1993) 52–59.
[38] A.O. De Souza, R.R. Santos-Jr, D.N. Sato, M.M.M. de Azevedo, D.A. Ferreira, P.S. Melo, M.H. Celio, L. Silva, N. Duranc, Journal of the Brazilian Chemical Society 15 (2004) 682–689.
[39] G.Y. Lee, K. Park, J.H. Nam, S.Y. Kim, Y. Byun, Journal of Drug Targeting 14 (2006) 707–716.